ACKNOWLEDGMENT

The computational resources and services used in this work were provided by the Hercules Foundation and the Flemish Government—Department EWI. Special thanks goes to K. Hoste and W. Depypere (HPC-UGent team) for their kind support.

REFERENCES

[1] W. C. Chew, J. Jin, E. Michielssen, and J. Song, *Fast and Efficient Algorithms in Computational Electromagnetics*. Boston, MA, USA: Artech House, 2001.

[2] S. Velamparambil, J. M. Song, W. C. Chew, and K. Gallivan, "ScaleME: a portable scaleable multipole engine for electromagnetic and acoustic integral equation solvers," in *Proc. IEEE Antennas and Propagation Soc. Int. Symp.*, 1998, vol. 3, pp. 1774–1777.

[3] P. Have, "A parallel implementation of the fast multipole method for maxwell's equations," *Int. J. Numer. Meth. Fluids*, vol. 43, no. 8, pp. 839–864, Nov. 2003.

[4] F. Wu, Y. Zhang, Z. Z. Oo, and E. Li, "Parallel multilevel fast multipole method for solving large-scale problems," *IEEE Antennas Propag. Mag.*, vol. 47, no. 4, pp. 110–118, Aug. 2005.

[5] J. Fostier and F. Olyslager, "An asynchronous parallel MLFMA for scattering at multiple dielectric objects," *IEEE Trans. Antennas Propag.*, vol. 56, no. 8, pp. 2346–2355, Aug. 2008.

[6] S. Velamparambil and W. C. Chew, "10 Million Unknowns: Is it that big?," *IEEE Antennas Propag. Mag.*, vol. 45, no. 2, pp. 43–58, Feb. 2003.

[7] S. Velamparambil and W. C. Chew, "Analysis and performance of a distributed memory multilevel fast multipole algorithm," *IEEE Trans. Antennas Propag.*, vol. 53, no. 8, pp. 2719–2727, Aug. 2005.

[8] Ö. Ergül and L. Gürel, "Hierarchical parallelisation strategy for multilevel fast multipole algorithm in computational electromagnetics," *Electron. Lett.*, vol. 44, no. 6, pp. 3–4, 2008.

[9] Ö. Ergül and L. Gürel, "A hierarchical partitioning strategy for an efficient parallelization of the multilevel fast multipole algorithm," *IEEE Trans. Antennas Propag.*, vol. 57, no. 6, pp. 1740–1750, Jun. 2009.

[10] L. Gürel and Ö. Ergül, "Hierarchical parallelization of the multilevel fast multipole algorithm (MLFMA)," *Proc. IEEE*, vol. 101, no. 2, pp. 332–341, 2013.

[11] C. Waltz, K. Sertel, M. A. Carr, B. C. Usner, and J. L. Volakis, "Massively parallel fast multipole method solutions of large electromagnetic scattering problems," *IEEE Trans. Antennas Propag.*, vol. 55, no. 6, pp. 1810–1816, 2007.

[12] J. M. Taboada, L. Landesa, F. Obelleiro, J. L. Rodriguez, J. M. Bertolo, M. G. Araujo, J. C. Mouriño, and A. Gomez, "High scalability FMM-FFT electromagnetic solver for supercomputer systems," *IEEE Antennas Propag. Mag.*, vol. 51, no. 6, pp. 20–28, 2009.

[13] V. Melapudi, B. Shanker, S. Seal, and S. Aluru, "A scalable parallel wideband MLFMA for efficient electromagnetic simulations on large scale clusters," *IEEE Trans. Antennas Propag.*, vol. 59, no. 7, pp. 2565–2577, Jul. 2011.

[14] B. Michiels, J. Fostier, I. Bogaert, and D. D. Zutter, "Weak scalability analysis of the distributed-memory parallel MLFMA," *IEEE Trans. Antennas Propag.*, vol. 61, no. 11, pp. 5567–5574, Nov. 2013.

[15] J. Fostier and F. Olyslager, "Provably scalable parallel multilevel fast multipole algorithm," *Electron. Lett.*, vol. 44, no. 19, pp. 1111–1112, Sep. 2008.

[16] X. M. Pan, W. C. Pi, M. L. Yang, Z. Peng, and X. Q. Sheng, "Solving problems with over one billion unknowns by the MLFMA," *IEEE Trans. Antennas Propag.*, vol. 60, no. 5, pp. 2571–2574, May 2012.

[17] F. Wei and A. Yilmaz, "A more scalable and efficient parallelization of the adaptive integral method—Part II: BIOEM application," *IEEE Trans. Antennas Propag.*, vol. 62, no. 2, pp. 727–738, Feb. 2014.

[18] G. Amdahl, "Validity of single-processor approach to achieving large-scale computing capability," in *Proc. AFIPS Conf.*, 1967, pp. 483–485.

[19] G. Mie, "Beiträge zur Optik tr über Medien, speziell kolloidaler Metallösungen," *Annalen der Physik*, vol. 25, no. 3, pp. 377–445, 1908.

[20] J. R. Mautz and R. F. Harrington, "H-field, E-field, and combined-field solutions for conducting bodies of revolution," *Archiv für Elektronik und Übertragungstechnik*, vol. 32, no. 4, pp. 157–164, Apr. 1978.

A Novel Low-Profile Hepta-Band Handset Antenna Using Modes Controlling Method

Changjiang Deng, Yue Li, Zhijun Zhang, and Zhenghe Feng

***Abstract*—It is a challenging and tough task to achieve and tune multiple frequencies for handset antennas in a small area. In this communication, we have proposed a novel modes controlling method to build and tune the handset antenna. By combining different modes of an open slot and different monopole branches, a hepta-band, covering GSM850, GSM900, DCS, PCS, UMTS, LTE2300, and LTE2500, handset antenna is achieved in a small area of 8×60 mm^2. The most essential merit of the proposed antenna is that the related modes can be added step by step, according to the operating bands. The modes for the lower and upper bands can be easily tuned and optimized. We have also built a prototype of the proposed antenna to validate the design strategy. The tested results include reflection coefficient, radiation patterns, efficiency, and gain.**

***Index Terms*—Handset antennas, multiple band antennas, modes controlling method.**

I. INTRODUCTION

With the rapid development of cellular communications, modern mobile handsets are required to support various wireless communication services. Accordingly, the mobile handset antenna should be multiband or broadband to provide sufficient bandwidth. However, the available space for antenna design in mobile handset is limited. Therefore, the conflicting considerations of multifunction and miniaturization lead to a continuous challenge in mobile handset antenna design.

To cover different operating kinds of modes, dual-band operation is usually required in the mobile handset. Monopole and slot antennas are the typical radiators for dual-band operation [1]–[3]. However, the bandwidth of a single radiator is narrow to cover the whole desired band. To obtain two wide bands while keeping a compact volume, various designs have been proposed. Frequency-reconfigurable antennas are an effective solution [4], [5], but the use of diodes increases the complexity of the design. Integrating multiple antennas in one structure is another attractive approach [6]–[14]. In this method, two or more resonances are generated in the lower band by different types of radiators, such as monopole, loop, PIFA, and slot. For example, a monopole antenna and an open slot antenna in [6], a loop antenna and an open slot antenna in [7], a PIFA antenna and an open slot antenna in [8], are integrated in a small volume. Nevertheless, the proposed antennas in [6]–[8] have a 3-D structure, which are not suitable for integration and slim design. Several on-board mobile handset antennas integrated with two radiators are proposed in [9]–[14]. For instance, two open slots in [9], an open slot and a short slot in [10], and a monopole and

Manuscript received May 13, 2014; revised October 28, 2014; accepted November 23, 2014. Date of publication December 08, 2014; date of current version January 30, 2015. This work was supported by the National Basic Research Program of China under Contract 2013CB329002, in part by the National Natural Science Foundation of China under Contract 61301001, the National Science and Technology Major Project of the Ministry of Science and Technology of China 2013ZX03003008-002, the China Postdoctoral Science Foundation funded project 2013M530046, and in part by the Beijing Excellent Doctoral Dissertation Instructor project 20131000307.

The authors are with the State Key Laboratory on Microwave and Digital Communications, Tsinghua National Laboratory for Information Science and Technology, Department of Electronic Engineering, Tsinghua University, Beijing, 100084, China (e-mail: lyee@tsinghua.edu.cn).

Color versions of one or more of the figures in this communication are available online at http://ieeexplore.ieee.org.

Digital Object Identifier 10.1109/TAP.2014.2378317

a parasitic strip in [11]–[14], are combined with a planar structure for multiple modes design.

However, the upper band of the antennas mentioned above is typically covered by the higher order of the radiators. The possible drawback of this method is that the tuning of the upper band is difficult, because the tuning of higher order usually affects the performance of the fundamental mode in the lower band. In a recent work [15], a hepta-band IFA with independent resonance control is presented. Four branches are used to generate four resonances. However, the volume is 3-D with $50 \times 10 \times 3$ mm^3 and a lumped inductor is adopted.

In this communication, monopole and open slot antennas are integrated in a planar structure, which features a low profile of 8 mm. The two 0.25λ modes of the monopole and the open slot are combined to cover the lower band. The two 0.75λ modes of the monopole and the open slot are also adopted to provide bandwidth for the upper band. To cover the whole upper band and have more freedom in tuning the bandwidth of upper band, two more resonances are added. A detailed parameter study is carried out, which shows that each mode in the lower and upper bands can be easily tuned. The measured results show that the bandwidth in the lower band covers GSM850 (824–894 MHz) and GSM900 (880–960 MHz), and the bandwidth in the upper band covers DCS (1710–1880 MHz), PCS (1850–1990 MHz), UMTS (1920–2170 MHz), LTE2300 (2305–2400 MHz) and LTE2500 (2500–2690 MHz).

II. Antenna Design

Fig. 1(a) shows the geometry of the proposed planar handset antenna, whose detailed dimensions are given in Fig. 1(b). A 0.8-mm-thick FR4 substrate ($\varepsilon_r = 4.4, \tan\delta = 0.02$) is used as the system circuit board. Three monopole-type branches are printed on the front side of the substrate. Branch #1 is a U-shaped strip, branch #2 is a straight strip, and branch #3 is an L-shaped strip. A tuning pad is connected to the longer arm of branch #1. The three branches are directly fed by a 50-Ω microstrip line. The ground plane is printed on the back side of the substrate. An open slot is etched on the ground plane with a length of 59 mm. The main ground, namely the part at one side of the slot, has a size of 100×60 mm^2. Another parasitic ground branch (branch #4) is placed at the other side of the slot. The detailed dimensions of the proposed antenna are optimized by using the commercial software Ansoft HFSS version 11.2.

The tuning process of the lower band is shown in Fig. 2. In the beginning, a folded monopole (branch #1) antenna is shown in Type I. The resonance of the monopole in the lower band is at about 990 MHz, corresponding to the 0.25λ mode of branch #1. Then, an open slot is etched on the ground plane in Type II. It is shown that another resonance in the lower band is generated at about 850 MHz. The resonance is corresponding to the 0.25λ mode of the open slot. Then, a tuning pad is added in Type III. Comparing Type III with Type II, it is shown that the 0.25λ mode of branch #1 is deceased. It can be explained that the tuning pad increases the current path length of the monopole. By merging the two modes, the coverage of GSM850/900 operation is achieved. It is worth mentioning that LTE700 operation can also be covered if the slot width or the monopole profile is increased, but this improvement will also increase the profile of the proposed antenna.

The tuning process of the upper band is shown in Fig. 3. In Type III, there are two resonances in the upper band, which correspond to the two 0.75λ modes of the open slot and the monopole. Then, branch #2 is added in Type IV. The main purpose of branch #2 is to tune the two 0.75λ modes. Considering that the bandwidth provided by the two 0.75λ modes is limited, additional resonances are required to cover the whole bandwidth in the upper band. Then, branch #4 is added in Type V to provide a new resonance. The branch operates at its 0.25λ mode and generates a resonance at about 2300 MHz. Finally, branch #3 is added in the proposed antenna to provide another resonance. The

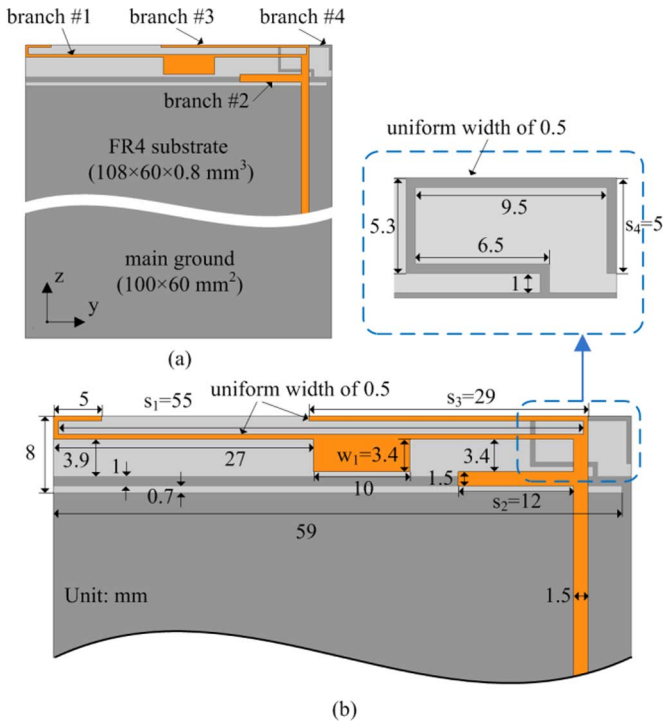

Fig. 1. (a) Geometry of the proposed antenna; (b) Dimensions of the proposed antenna.

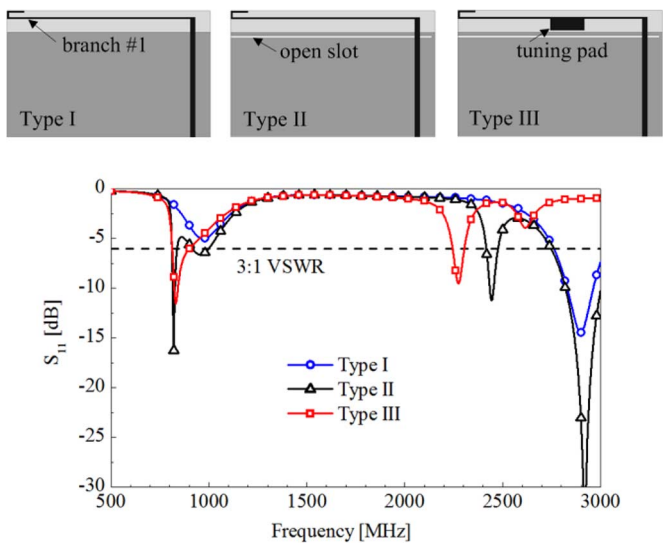

Fig. 2. Comparison of simulated S_{11} for different antenna types. Type I: only branch #1, Type II: Type I + open slot, Type III: Type II + tuning pad.

branch operates at its 0.25λ mode and generates a resonance at about 1800 MHz. It is shown that branch #3 can also tune the whole upper band effectively. By merging the four modes, the coverage of the upper band is achieved.

Fig. 4 compares the simulated input impedance of three typical antennas. It is observed that the monopole in Type I generates a resonance at about 990 MHz in the lower band. By applying the coupling feed, the open slot is excited and an additional resonance is provided at about 850 MHz in Type IV. The comparison of the two antennas indicates the mechanism of feeding in the lower band. Based on Type IV, the proposed antenna has an additional monopole branch and ground strip. It is shown that two more resonances in the upper band are excited in the

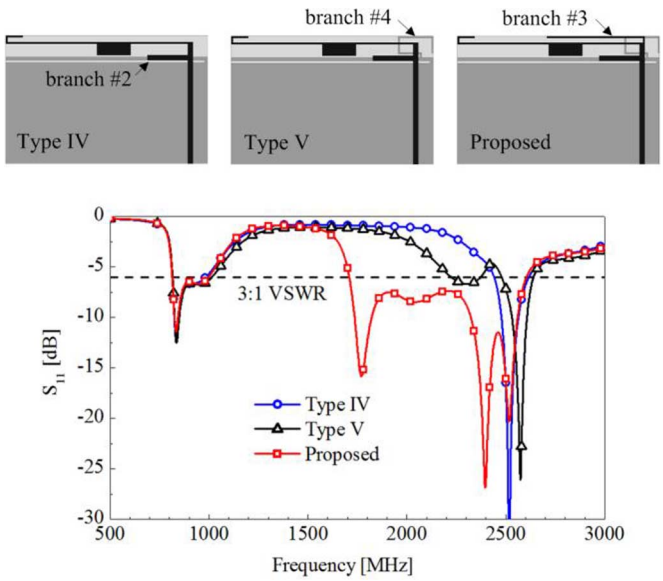

Fig. 3. Comparison of simulated S_{11} for different antenna types. Type IV: Type III + branch #2, Type V: Type IV + branch #4, proposed: Type V+ branch #3.

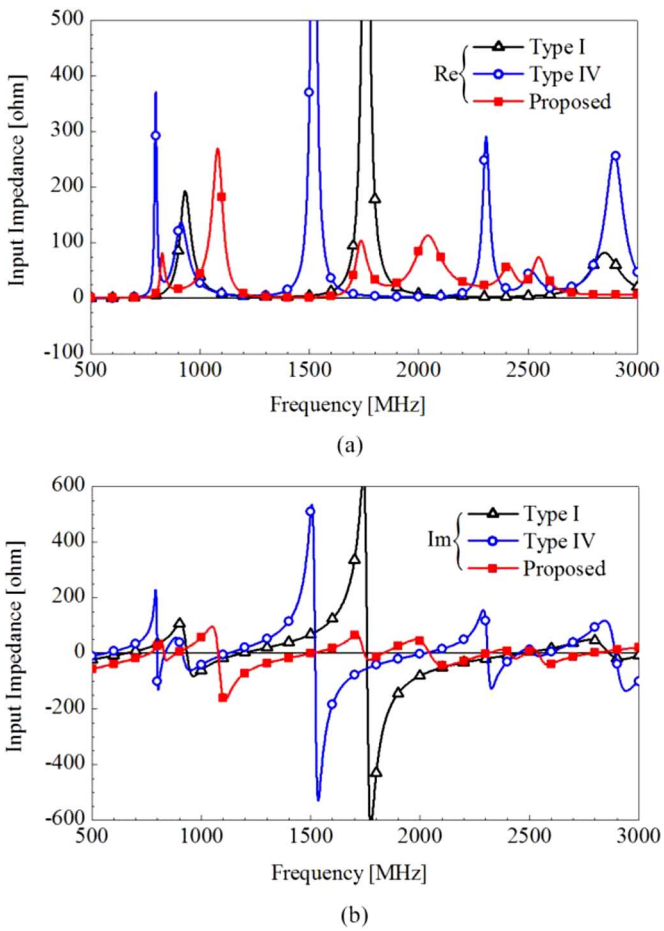

Fig. 4. Simulated input impedance of the proposed antenna. (a) resistance; (b) reactance.

proposed antenna. The comparison of the two antennas indicates the mechanism of feeding in the upper band.

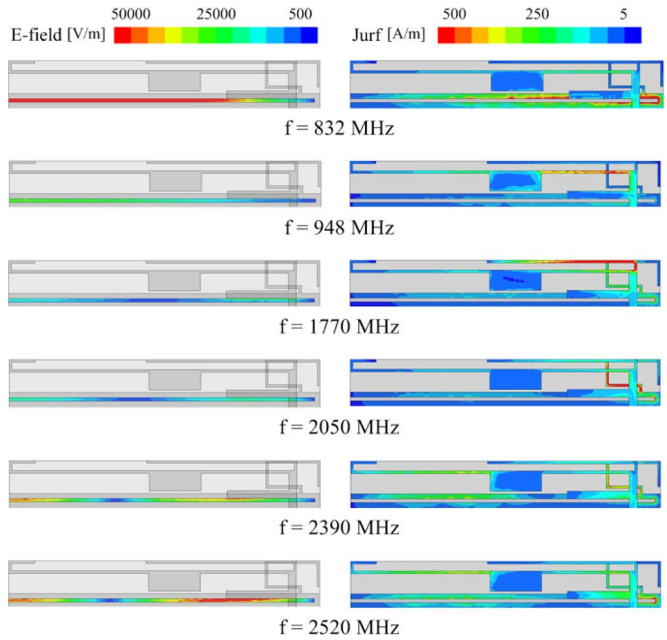

Fig. 5. Simulated distribution of the electric field in the open slot and the surface current of the proposed antenna.

The simulated distribution of the electric field [16] and the surface current at different resonant frequencies are shown in Fig. 5. The corresponding radiating antenna part for each resonant mode is clearly shown. To be specific, the resonance at 832 MHz is generated by the open slot, the resonance at 948 MHz is generated by branch #1, the resonances at 1770 MHz and 2050 MHz are generated by branch #3 and branch #4, and the resonances at 2390 MHz and 2520 MHz are generated by the third-order modes of branch #1 and the open slot.

III. Parameter Study

As the lower band is difficult to cover, the key parameters for the lower band are studied first. There are two resonances in the lower band, which are generated by branch #1 and the open slot. Therefore, the lengths of branch #1 and the open slot are the key factors to tune the two modes. Fig. 6 shows the simulated S_{11} with different lengths of branch #1. It is shown that increasing s_1 can both decrease the 0.25λ mode and 0.75λ mode of branch #1. However, the length of branch #1 is limited by the width of the ground plane. Therefore, a tuning pad is added to further decrease the 0.25λ mode of branch #1. It is shown in Fig. 7 that the 0.25λ mode of branch #1 decreases with the increase of the tuning pad width w_1. Besides, the two 0.75λ modes of branch #1 and the open slot also decrease with the increase of w_1. It can be explained that the tuning pad works as a shunt capacitor. These results clearly indicate that the lower band can be effectively controlled by tuning the length of branch #1 and the tuning pad width.

The key parameters for the upper band are also studied. There are four resonances in the upper band, namely the 0.75λ mode of the open slot, the 0.75λ mode of branch #1, the 0.25λ mode of branch #3, and the 0.25λ mode of branch #4. As the lengths of branch #1 and the open slot are used to tune the 0.25λ modes, an alternative parameter is found to tune the two 0.75λ modes. Fig. 8 shows the effect of branch #2. When s_2 increases, the third-order mode of branch #1 decreases but the third-order mode of the open slot increases. Fig. 9 shows that branch #3 only affects the resonance at 1800 MHz. A similar phenomenon can be found in Fig. 10, where the resonance is determined by branch #4. It is worth mentioning that the two resonances in the lower band keep almost unchanged during the parameter tuning of the upper band.

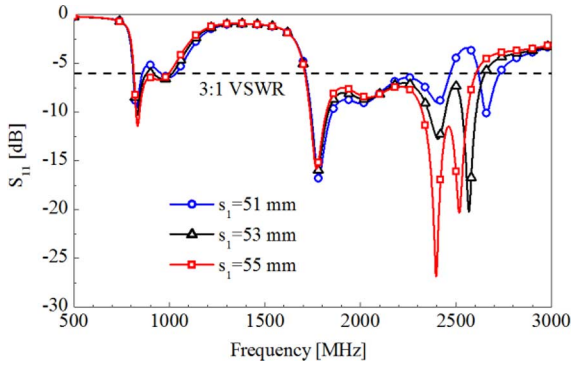

Fig. 6. Simulated S_{11} with different lengths of branch #1.

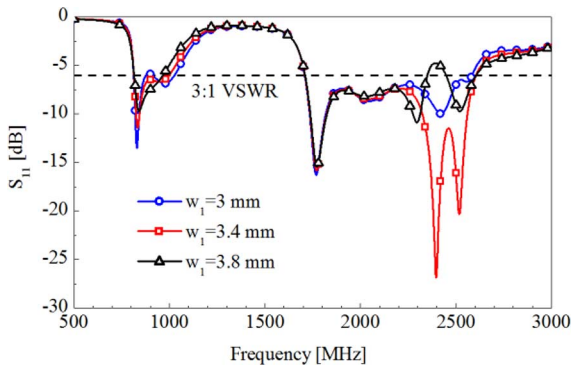

Fig. 7. Simulated S_{11} with different widths of the tuning pad.

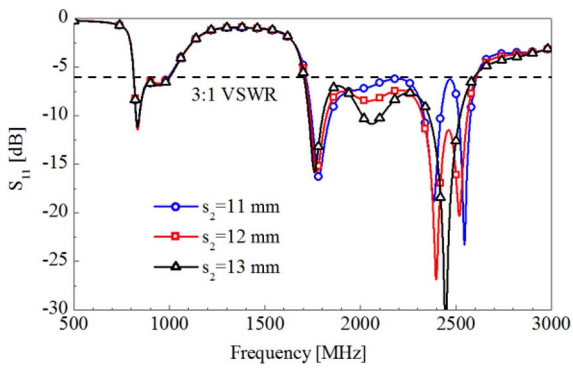

Fig. 8. Simulated S_{11} with different lengths of branch #2.

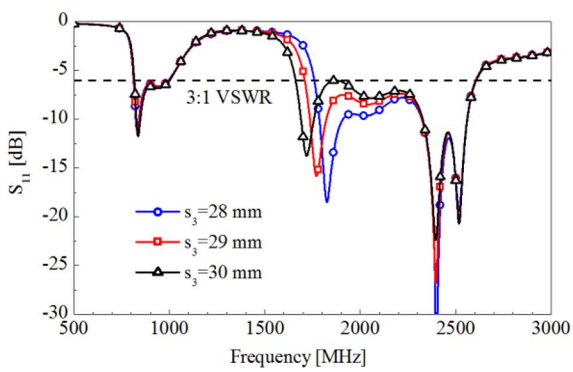

Fig. 9. Simulated S_{11} with different lengths of branch #3.

These results indicate that the four modes in the upper band can be tuned easily.

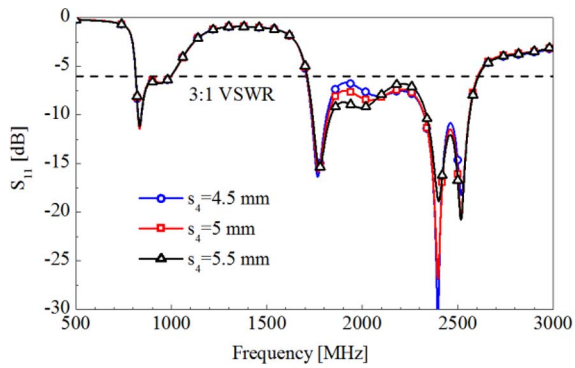

Fig. 10. Simulated S_{11} with different lengths of branch #4.

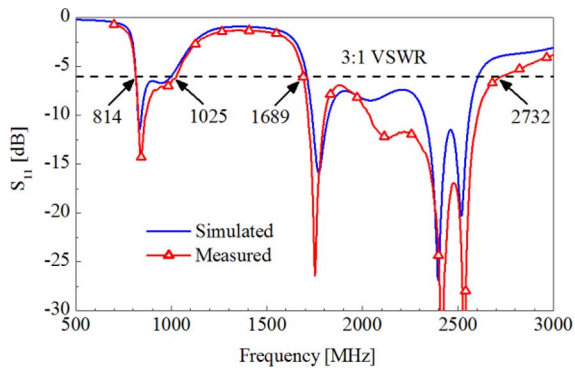

Fig. 11. Simulated and measured S_{11} of the proposed antenna.

IV. Experimental Results

Based on the optimized parameters in Fig. 1, a prototype of the proposed antenna is fabricated. Fig. 11 shows the simulated and measured reflection coefficients of the proposed antenna. The difference between simulation and measurement is mainly caused by fabrication error and substrate property. Two resonances are observed in the lower band, and a bandwidth of 205 MHz (815–1020 MHz) is achieved, which covers the GSM850, GSM900 operations. Four resonances are observed in the upper band, and a bandwidth of 1040 MHz (1690–2730 MHz) is achieved, which covers DCS, PCS, UMTS, LTE2300 and LTE2500 operations.

The normalized radiation patterns of the proposed antenna are shown in Fig. 12. For the lower frequency 900 MHz, a dipole-like radiation pattern can be observed. For the upper frequencies 1900 MHz and 2400 MHz, more variations and nulls appear in the patterns when compared with that at 900 MHz. The simulated and measured gain and efficiency in the lower and upper bands are presented in Figs. 13 and 14, respectively. For the lower band, the radiation efficiency is larger than 40% and the antenna gain varies from -2 to 1 dBi. For the upper band, the radiation efficiency is about 44–70%, and the antenna gain varies from -2 to 2 dBi. The results deteriorate at the boundary of the concerned band, but are acceptable in practical mobile applications.

The SAR results are studied in Fig. 15. The SAR simulation model is built with SEMCAD tool. The proposed antenna is placed at the bottom of the system circuit board. The board is close to the head ear with a distance of 5 mm and is inclined to the vertical line with 60°. The input power is 24 dBm for GSM850/900 operation and 21 dBm for GSM1800/1900, UMTS and LTE operation. It is shown that the simulated SAR values are all well below the SAR limit of 1.6 W/kg, which indicates that the proposed antenna is promising in mobile applications.

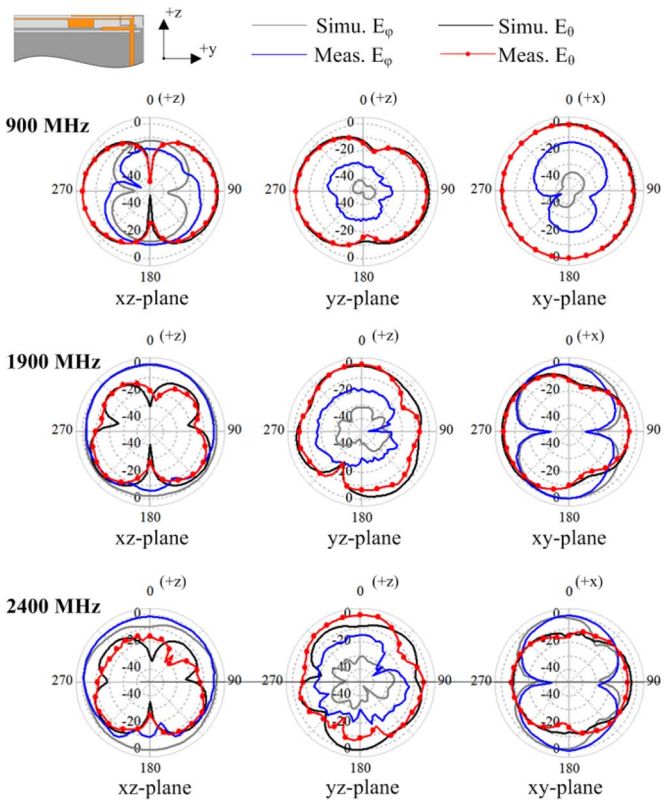

Fig. 12. Simulated and measured radiation patterns of the proposed antenna.

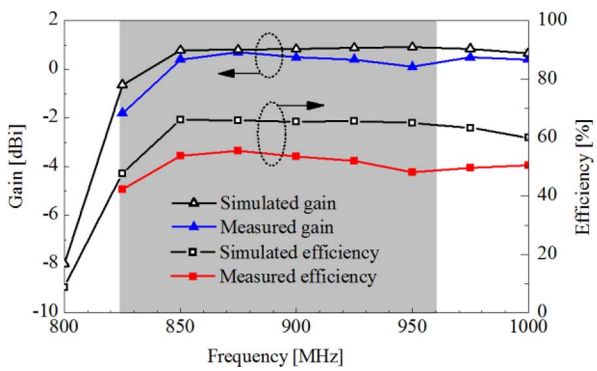

Fig. 13. Simulated and measured gain and efficiency in the lower band.

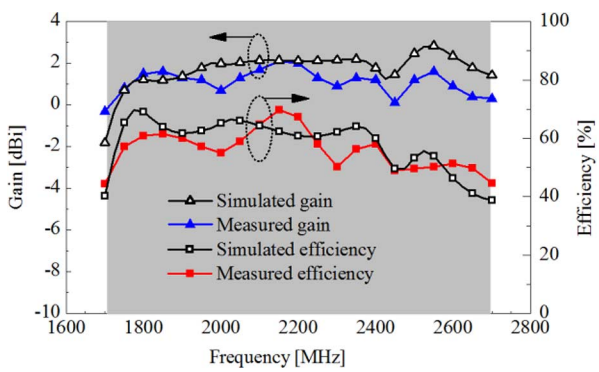

Fig. 14. Simulated and measured gain and efficiency in the upper band.

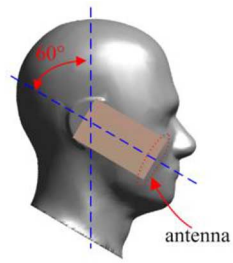

Frequency (MHz)	859	925	1795	1920	2045	2350	2595
1-g SAR (W/kg)	1.02	1.19	0.35	0.34	0.36	0.33	0.43
Return loss (dB)	7.7	6.2	12.8	7.35	8.22	11.2	6.93

Fig. 15. SAR simulation model and the SAR values for 1-g head tissues.

V. Conclusion

In this communication, a compact planar handset antenna for multi-band operation has been proposed. The proposed antenna occupies a small area of 8×60 mm^2, featuring a low profile of 8 mm. Different modes of the open slot and different monopole branches are excited and optimized. The 0.25λ mode of branch #1 and the 0.25λ mode of the open slot are combined to cover the GSM850, GSM900 operations in the lower band. The 0.75λ mode of branch #1, the 0.75λ mode of the open slot, the 0.25λ mode of branch #3, and the 0.25λ mode of branch #4 are combined to cover the DCS, PCS, UMTS, LTE2300, and LTE2500 operations in the upper band. The advantages of low profile and ease of modes control enable the proposed antenna to have potential usage in mobile applications.

References

[1] K. L. Wong, G. Y. Lee, and T. W. Chiou, "A low-profile planar monopole antenna for multiband operation of mobile handsets," *IEEE Trans. Antennas Propag.*, vol. 51, pp. 121–125, 2003.

[2] Y. L. Ban, C. L. Liu, J. L. W. Li, and R. Li, "Small-size wideband monopole with distributed inductive strip for seven-band WWAN/LTE mobile phone," *IEEE Antennas Wireless Propag. Lett.*, vol. 12, pp. 7–10, 2013.

[3] C. I. Lin and K. L. Wong, "Printed monopole slot antenna for internal multiband mobile phone antenna," *IEEE Trans. Antennas Propag.*, vol. 55, no. 12, pp. 3690–3697, Dec. 2007.

[4] Y. Li, Z. Zhang, W. Chen, Z. Feng, and M. F. Iskander, "A quad-band antenna with reconfigurable feedings," *IEEE Antennas Wireless Propag. Lett.*, vol. 8, pp. 1069–1071, 2009.

[5] Y. Li, Z. Zhang, J. Zheng, Z. Feng, and M. Iskander, "A compact hept-aband loop-inverted F reconfigurable antenna for mobile phone," *IEEE Trans. Antennas Propag.*, vol. 60, no. 1, pp. 389–392, Jan. 2012.

[6] C. Lin and K. L. Wong, "Internal hybrid antenna for multiband operation in the mobile phone," *Microw. Opt. Tech. Lett.*, vol. 50, no. 1, pp. 38–42, Jan. 2008.

[7] C. H. Wu and K. L. Wong, "Internal hybrid loop/monopole slot antenna for quad-band operation in the mobile phone," *Microw. Opt. Technol. Lett.*, vol. 50, pp. 795–801, Mar. 2008.

[8] J. Anguera, I. Sanz, J. Mumbru, and C. Puente, "Multiband handset antenna with a parallel excitation of PIFA and slot radiators," *IEEE Trans. Antennas Propag.*, vol. 58, no. 2, pp. 348–356, Feb. 2010.

[9] K. L. Wong and L. C. Lee, "Multiband printed monopole slot antenna for WWAN operation in the laptop computer," *IEEE Trans. Antennas Propag.*, vol. 57, pp. 324–330, Feb. 2009.

[10] C. H. Wu and K. L. Wong, "Hexa-band internal printed slot antenna for mobile phone application," *Microw. Opt. Technol. Lett.*, vol. 50, pp. 35–38, Jan. 2008.

[11] F. H. Chu and K. L. Wong, "Planar printed strip monopole with a closely-coupled parasitic shorted strip for eight-band LTE/GSM/UMTS mobile phone," *IEEE Trans. Antennas Propag.*, vol. 58, pp. 3426–3431, Oct. 2010.

[12] S. Wang and Z. Du, "A compact octaband printed antenna for mobile handsets," *IEEE Antennas Wireless Propag. Lett.*, vol. 12, pp. 1347–1350, 2013.
[13] Y. L. Ban, C. L. Liu, J. L. W. Li, J. H. Guo, and Y. J. Kang, "Small-size coupled-fed antenna with two printed distributed inductors for seven band WWAN/LTE mobile handset," *IEEE Trans. Antennas Propag.*, vol. 61, no. 11, pp. 5780–5784, Nov. 2013.
[14] Y. L. Ban, Y. F. Qiang, Z. Chen, K. Kang, and J. L. Li, "Low-profile narrow-frame antenna for seven-band WWAN/LTE smartphone applications," *IEEE Antennas Wireless Propag. Lett.*, vol. 13, pp. 463–466, 2014.
[15] J. Lee and Y. Sung, "Heptaband inverted-F antenna with independent resonance control for mobile handset applications," *IEEE Antennas Wireless Propag. Lett.*, vol. 13, pp. 1267–1270, 2014.
[16] K. L. Wong, W. J. Chen, L. C. Chou, and M. R. Hsu, "Bandwidth enhancement of the small-size internal laptop computer antenna using a parasitic open slot for penta-band WWAN operation," *IEEE Trans. Antennas Propag.*, vol. 58, no. 10, pp. 3431–3435, 2010.

An Accurate Conformal Fourier Transform Method for 3D Discontinuous Functions

Chunhui Zhu, Qing Huo Liu, Lijun Liu, and Yanhui Liu

***Abstract*—Fourier transform of discontinuous functions are often encountered in computational electromagnetics and other areas. In this work, a highly accurate, fast conformal Fourier transform (CFT) algorithm is proposed to evaluate the finite Fourier transform of 3D discontinuous functions. A curved tetrahedron mesh combined with curvilinear coordinate transform, instead of the Cartesian grid, is adopted to flexibly model an arbitrary shape of the discontinuity boundary. This enables us to take full advantages of high order interpolation and Gaussian quadrature methods to achieve highly accurate Fourier integration results with a low sampling density. The 3D nonuniform fast Fourier transform (NUFFT) helps to keep the complexity of the proposed algorithm to that similar to the traditional 3D FFT algorithm. Therefore, the proposed CFT algorithm can achieve order of magnitude higher accuracy than 3D FFT with lower sampling density and similar computation time. The convergence is proved and verified.**

***Index Terms*—3D, conformal Fourier transform, discontinuous functions, nonuniform fast Fourier transform.**

I. Introduction

Fourier transform (FT), as a most important tool for spectral analyses, is often encountered in computational physics, including areas such as electromagnetics [1]–[4], image processing [5], [6] and acoustics [7], [8].

The traditional fast Fourier transform (FFT) algorithm is the most popular approach to evaluate the Fourier transform. In practice, however, many functions to be transformed are discontinuous across the boundary of an irregular area. For example, in volume integral equation solvers in electromagnetics, some components of the unknown electric current density to be transformed are discontinuous across the material interfaces, which in general have arbitrary shapes [9], [10]. For this kind of functions, however, there usually exist significant stair-casing errors due to the uniform Cartesian orthogonal grid required by the traditional high dimensional FFT algorithm, and the accuracy is limited since FFT is based on the trapezoidal quadrature scheme.

Some works have been done to improve the accuracy for one-dimension (1D) piecewise smooth functions [9], [11]–[16]. 1D CFT method has been applied to solve the volume integral equations in electromagnetics, and obtain results of 50 dB more accurate than using FFT with comparable computation time [3]. Direct extension of these algorithms to high dimensions still requires that the area is meshed into a Cartesian orthogonal grid [9], which is not flexible for an arbitrary boundary shape. Recently, a conformal Fourier transform (CFT) algorithm has been proposed for 2D discontinuous functions in [10], [17] to allow an arbitrary boundary shape. As an extension of the 2D CFT, this work develops the conformal Fourier transform algorithm for 3D discontinuous functions distributing in a volume with an arbitrary boundary shape. The techniques of meshing 3D domain with tetrahedron elements, Lagrange interpolation and Gaussian quadrature on a tetrahedron elements, and curvilinear coordinate transform for a curved tetrahedron are used. With this 3D work, the CFT method is made to be a more complete one that is more useful in application.

The complexity of the proposed algorithm is $O(\mu^3 N_1 N_2 N_3 \log(\mu^3 N_1 N_2 N_3) + MQ^3)$, which is similar to the traditional 3D FFT algorithm, where $M = LI$; L is the number of the tetrahedron elements and I is the number of the quadrature points in each element. N_1, N_2 and N_3 are the numbers of sampling points in the frequency domain in each dimension, μ is the over-sampling factor in NUFFT, and $Q \ll \max(N_1, N_2, N_3)$ is a constant. The convergence is proved and are verified by numerical results. Numerical results also illustrate the advantages of the developed algorithm over the traditional 3D FFT algorithm.

II. Formulations and Algorithms

The objective of this work is to develop a fast and accurate algorithm for evaluating $F(u, v, w)$, the finite Fourier transform of a 3D piecewise smooth function $f(x, y, z)$,

$$F(u,v,w) = \int_V f(x,y,z) e^{j2\pi(ux+vy+wz)} dxdydz \qquad (1)$$

where $V = \bigcup_{i=1}^{I_v} V_i$ is composed of some finite 3D region V_i with arbitrary shapes, and $f(x, y, z)$ is continuous within each V_i.

In this section the tools used are first introduced and then the 3D conformal Fourier transform (3D CFT) algorithm is formulated.

A. Interpolation Over a Tetrahedron

When using the traditional 3D FFT algorithm to evaluate the integration (1), a uniform Cartesian orthogonal grid is required. This grid cannot describe very well the boundary shape of an arbitrary finite volume V_i, unless V_i is a cuboid with all sides parallel to coordinate

Manuscript received March 22, 2014; revised September 05, 2014; accepted November 23, 2014. Date of publication December 08, 2014; date of current version January 30, 2015. This work is supported in part by the National Natural Science Foundation of China (NSFC) under Grants 61301008, 61304110, and 61301009, and in part by the Fundamental Research Funds for the Central Universities under Grants 2012121036 and 10120131072. *(Corresponding author: L. Liu.)*

C. Zhu and Y. Liu are with the Department of Electronic Science, Xiamen University, Xiamen 361005, China (e-mail: zhuchhxd@xmu.edu.cn; yanhuiliu@xmu.edu.cn).

Q. H. Liu is with the Department of Electrical and Computer Engineering, Duke University, Durham, NC 27708 USA (e-mail: qhl@duke.edu).

L. J. Liu is with the Department of Automation, Xiamen University, Xiamen 361005, China (e-mail: liulijun@xmu.edu.cn).

Color versions of one or more of the figures in this communication are available online at http://ieeexplore.ieee.org.

Digital Object Identifier 10.1109/TAP.2014.2378315